A NEW DATA ACQUISITION DESIGN FOR BREAST CANCER DETECTION SYSTEM

Dung Nguyen[1], Kui Ren[2], Janet Roveda[1]

[1]Department of Electrical and Computer Engineering,
University of Arizona at Tucson
Tucson, AZ 85721, USA
[2]Department of Computer Science and Engineering
University at Buffalo, State University of New York (SUNY)
Buffalo, New York 14260, USA

ABSTRACT

Modern mammography screening for breast cancer detection adopted computed tomography techniques and multi-dimensional (i.e. 3D or 4D) Tomosynthesis to improve cancer detection rate. These new trends demand novel SoC designs that can accommodate the increasing volume of raw data from multi-dimensional (i.e. 3D or 4D) Tomosynthesis with comparable X-ray dose. The current paper introduces two core technologies: Adaptive Digital Estimator (ADE) and Self-detecting sensory array based on Compressive Sensing (CS) concept and inter-reset sampling techniques. First of its kind, the new designs can simultaneously achieve high speed data acquisition and reduce data amount by an average of 40%.

I. INTRODUCTION

Breast cancer is a leading cause of cancer mortality in women around the world, especially for women in the 35-59 age group[1]. According to the American Cancer Society datasheet[2], in US alone, one out of eight women (12%) will have invasive breast cancer some time during her lifetime and about one in thirty-three will die of this disease. The key approach to improve the surviving rate is early detection and treatment. For instance, the five-year survival rate of diagnosed cases is nearly 100%, when cancer is confined to breast ducts. Early detection of breast cancer minimizes body pain and suffering, and allows patients to continue with their normal lives. Currently, the conventional 2D mammography is the most popular approach to detect early stage breast cancer. However, it is well-known that the 2D mammography has limitations in detecting breast cancers: a recent report shows that it misses 10% to 30% of breast tumors [3] due to anatomical noises, caused by the overlaps of breast tissues under 2D projections. One effective way to avoid anatomical noises is by using higher dimensional approaches, i.e. 3D and 4D Breast Computed Tomography (Breast CT) [4] and Tomosynthesis. Still, the major challenge is the dramatic increase in the data volume: for 3D Breast CT and Tomosynthesis, 15 frames of images are required comparing with 2 frames for the traditional 2D ones. This is equivalent to 7X increase in data volume. In addition, there will be increase in X-ray dose as well. If we implement both 2D and 3D Breast CT and Tomosynthesis using full field digital mammography (FFDM), 3D approaches will have 8% increase in X-ray dose comparing with 2D ones for normal density breasts. For high density breasts, the increased amount can be as high as 83% [5]. Figure 1 demonstrates the proposed architecture of this new design. Note that different from traditional digital X-ray system, the proposed one targets a new generation of biomedical instrument designs. The new design is mobile, low memory storage, and cloud based. For example, X-rays going through human tissues arrive at pixel array (sensor array in the figure). The grey circle covered area indicates the new SoC design circuit and its components. The proposed system propagates image through buffers, the designed circuits and then send out the output to cloud to perform image reconstruction. The new design is consistent with the new concept on big data and cloud computing.

978-1-4799-1166-0/13/$31.00 ©2013 IEEE

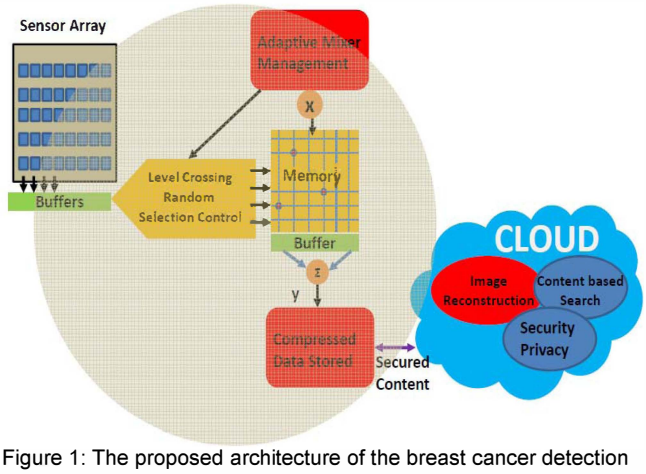

Figure 1: The proposed architecture of the breast cancer detection system.

The contributions of this paper can be summarized as follows. We developed a level crossing sampling approach to replace Nyquist samplings in the current SoC system. A new front end circuit that combines the level crossing concept with random selection matrix is integrated into this design. The new Adaptive Digital Estimator (ADE) design employs level crossing and compressive sensing kernels to improve Signal and Noise Ratio (SNR) with less data. This is very different from prior approaches that use the analog multipliers, floating gates, mixer generators and Analog Digital Converters to reduce the data amount [6][7]. In addition, the proposed Inter-Reset Sampling (IRS) makes it possible to have multiple frames of images between two resets of Pixel array. This new technique further reduces X-ray does. The new circuit performs digitization only when there is enough variation in the input and when the random selection matrix chooses this input. We introduced self-test and self-tuning schemes into the current prototype monitoring systems. The new designs detect system errors and tune voltage and frequency on-the-fly. Once combined with correspondent mixer functions and random selection matrix, we expect to compensate system errors on line with the help of CS algorithms.

II. COMPRESSIVE SENSING CONCEPT

To understand the proposed circuits, let us first review Compressive sensing (CS), a newly invented idea for data compression. Different from JPEG and other data compression techniques, CS intends to only obtain the effective samples at the very beginning though random selection. Other tools such as JPEG first obtain as much as possible samples, and then perform data compression to throw out non-important ones. One most important property of CS is that it unanimously reduces the data amount throughout the whole system. The first application of CS in medical image processing was by [17-21] for reconstructing the corrupted Shepp-Logan Phantom. Compressed sensing technology was also used in clinical MRI by Michael Lustig in 2009. The requirement of Compressive Sensing (CS) is that an image is sparse (for example, only a few wavelet coefficients are significant). Then we can recover this image with limited measured data (for example, less than the Nyquist sampling rate) [26]. In the breast cancer mammogram application, this is not a problem, as the key features in the images we care about are tumor cells and calcification points. Both types are from different from the rest of the tissues and are sparsely distributed among healthy tissues. Mathematically, the CS framework can be formulated as: $\mathbf{y} = \mathbf{\Phi x}$, where $\mathbf{y}$ represents a measurement vector, $\mathbf{\Phi}$ is the random selection based sensing matrix, and $\mathbf{x}$ represents the original input signals being measured (i.e. the pixel array values). For example, the measured image using pixel array has N column vectors which are multiplied with pseudo-random vector projections. The result is a set of compact vectors with M columns where M << N.

III. ADAPTIVE DIGITAL ESTIMATOR DESIGN

This section focuses on new circuit designs and architectures to enable CS based fast data acquisition. We first introduce *Level Crossing based Random Selection*, a new concept that combines both level crossing sampling with the compressive sensing's random selection. Then, an adaptive design is introduced that allows the improvement of on-line sensing accuracy and the flexibility of voltage regulation to achieve trade-offs between low power and low error rate. Level Crossing based Random Selection is introduced to quantize the prior knowledge of voltage level and mixing functions or random selection matrices. This new scheme is different from the regular Nyquist sampling theorem and the level-crossing

ones. To illustrate, let us first discuss the difference between the Nyquist scheme and the level-crossing one. Refer to Figure 2 (a)-(c). Figure 2(a) is the regular Nyquist sampling scheme where a clock with period Tclk is applied to control when the sampling should happen [12]. Figure 2(b) displays the level-crossing sampling scheme [12]. Here a sample is accepted only if the input signal crosses one of the predefined voltage levels equally spaced with ΔV. Contrary to the Nyquist sampling data points, the time passed between two samples (refer to A and B points and ΔT in Figure 2(b)) depends on the signal variations instead of the clock period. Figure 2 (c) demonstrates the proposed level-crossing based random selection. In addition to the level-crossing, we only perform sampling when the random selection matrix would randomly select this sample. For example, if V2 is significantly different from V1, the level-crossing scheme shows that this is a potential new sampling point. However, if the random selection matrix has zero value with regard to this particular sample point, we would bypass it. Therefore, a sample is taken only if it is different from the previous sample point and it is randomly selected. Pixel data once created and buffered is not time sensitive. This is because the charge representing each pixel's grey level is not time dependant. Thus, level crossing based sampling provides a better and more suitable choice.

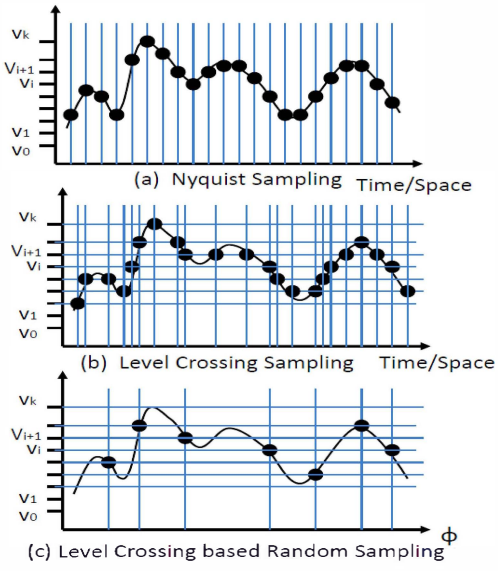

Figure 2: Different Sampling Schemes .

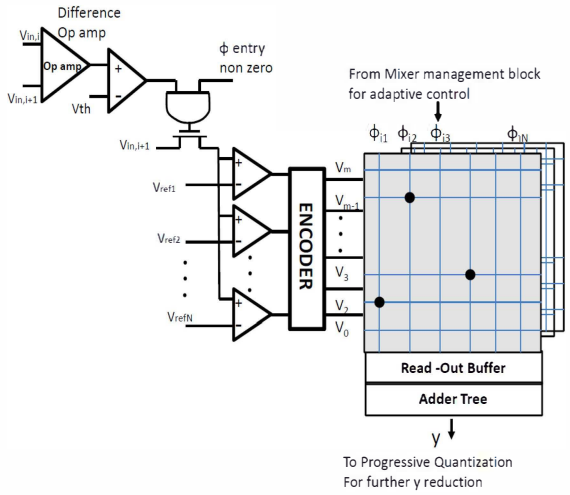

Figure 3: The proposed circuit design for level crossing based random sampling.

We propose a two-stage architecture for this new concept (refer to Figure 3). The first stage consists of a difference amplifier and a comparator. The difference amplifier captures signal variations. The reference voltage of the comparator is a predefined threshold voltage Vth. The second stage is a comparator array. The core component of this architecture is a set of memory array that stores the pre-calculated multiplication results of voltage levels and random selection matrix. Each entry of this memory array is the product of different voltage levels with random selection matrix entries. If the input signal difference exceeds the threshold voltage and the correspondent entry of random selection matrix is non-zero, we proceed with the second stage: the comparator array. Thus, this input signal sample point is digitized and then access the correspond product of the pre-stored memory array to get the product of this voltage level with the random selection matrix entry. If the random selection entry is zero, or the signal voltage is close to zero, or the signal variation is small, we bypass the comparator array. An adder is placed at the output of the memory access to compute compressed sensing measurements y. There are three advantages of this proposed sampling scheme. First of all, the sample rate of this proposed scheme depends on the sparsity of the signal, the sparsity of random selection matrix and the signal variations. We believe this sample rate is much lower than the Nyquist sampling rate.

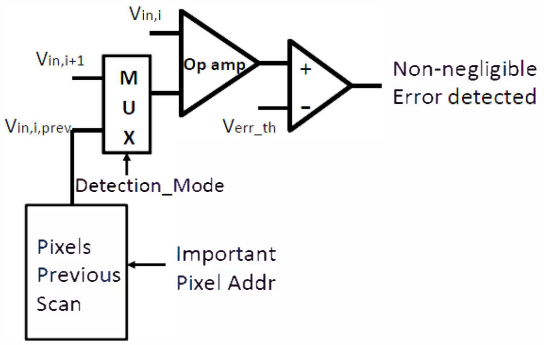

Figure 4: The self-detect architecture for the sensor array design.

Second, the majority of this design only uses digital components: memory, bypass control blocks, address encoder and adders. The access time of memory blocks are much higher than the analog multipliers. Parallel schemes can be easily applied here to improve the memory access speed. Finally, the random selection happens right after the quantization of the input signal, it may improve the digital quantization introduced error. This is contrary to the general compressive sensing scheme where quantization happens after we generate y.

Due to the inhomogenity and process variations in the manufacture procedure, we have varying sizes, positions and temperature sensitivities of CMOS transistors inside image sensors. These changes can lead to performance significantly different from the original design. For example, one of the major image degradations is the increasing fixed pattern noise in the CMOS image sensors [8][9][10][11][13]. The proposed self-detection structure constitutes a scan line, a control block to generate "detect mode" signal, a set of logic gates that detect the difference between two signals, and a signal correction block that reset the pixel data to correct one. Figure 4 shows the proposed self-detection structure. Instead of comparing two different pixels at different location, the "detect mode" requests the difference amplifier to compare the data from the same pixel at the first scan and the second scan (i.e. we consider images from X-ray, MRI, etc). If the difference exceeds the pre-set threshold, it is considered as significant. This self-detection structure requires storage units to store the pixel value from the first scan. Different from other existing self-detection and correction circuits

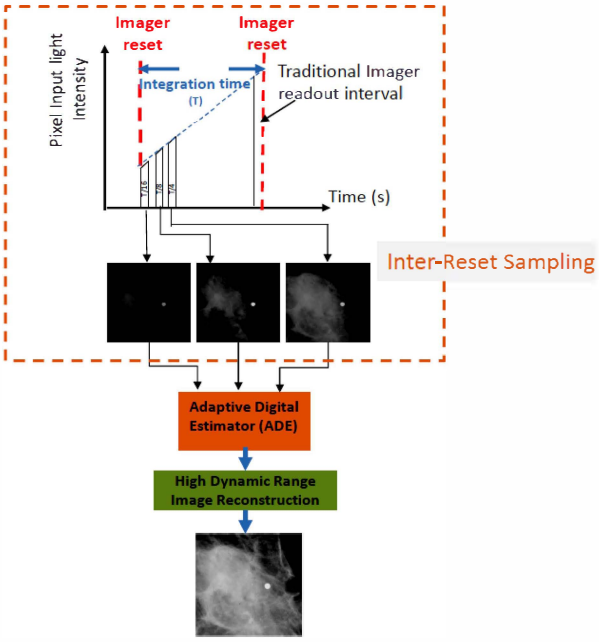

Figure 5: Circuit Connections between IRS and ADE.

[14][15], the proposed new structure fully utilizes the compressive sensing impact on signal corrections in the following three ways. First, during detection mode, not all pixels are self-compared. Only the ones that have major contributions to diagnostic results are selected. For example, in breast cancer detection, some pixels hold information of calcification spots. Others only contain background information. As we use compressive sensing to reconstruct the first scan image already, we know which pixels are more important than the others. Second, the level cross circuit automatically provides the structure to compare pixel's analog value given a temporary storage for the first scan pixels. Third, using adaptively changing mixers or random selection matrices, we can minimize detected pixel errors on the fly. The main cost of this implementation is in the storage units for first scan pixel data. The other circuitry is only less than 10% of the storage units in terms of both area cost and power consumptions.

IV. INTER-RESET SAMPLING DESIGN

Instead of the traditional "one reset one frame" approaches, the new Inter-reset Sampling design is able to take in several images during the two

adjacent resets of the image sensor. From the circuit design point of view, the "Non-destructive" input pin of one image sensor is first activated, which prohibits the pixel reset after the readout. Then the X-ray is turn on. The proposed Inter-Reset Sample (IRS) activates the Image Read input pin on the sensor at T/16, T/8 and T/4 where T is the integration time for the input pixel as charge. These images will be temporary stores in the cassette frame buffer. After the readout of T/4 image is completed, the X-ray is turn off. Figure 5 describes the flow chart of the proposed system. At the points of the inter-reset time, the three low exposure images at T/16, T/8 and T/4 need to align by the High Dynamic Range Image Reconstruction Support hardware (should locate at the boundary of Inter-Reset Sampling block, not shown explicitly in Figure 5). This support circuit is synthesized by using FPGA through stream code. In addition, we incorporate the Maximum A Posteriori (MAP) estimation algorithm for image reconstruction in the support circuit. After the image alignment, the preliminary high dynamic range image and the Maximum A Posteriori produced data file are the inputs to the Adaptive Digital Estimator (Orange Block in Figure 5). The reconstruction (in Green block) recovers the image based on the three low exposure ones.

IV. EXPERIMENTAL RESULTS

Breast images have different pixel ranges (0 to 4000) compared with lung images (0 to 25000). After checking and learning from many images (for example at database and Cloud) using content based search, it may draw the conclusion that the breast images require 12 bit quantization while the lung images require 15 bit quantization. This one bit difference leads to 87.5% reduction in the number of comparators (12 bit requires 2^{12} comparators, while 15 bit requires 2^{15} comparators), which in turn greatly reduces the power consumption at the comparator array. Additional studies on a large number of breast cancer images would reveal that dense breast tissues lead to lower pixel values. While the higher pixel values contains information about calcification spots (white spots in the mammographic images), this means we should focus on the accuracy of higher voltage level of the comparators. It is possible to reuse the lower voltage level comparators to refine lower voltage level to improve the resolution. To summarize, through cloud enabled search, we could have a better understanding of the design metrics in terms of power consumption, hardware cost and image quality specifications for different applications. Thus, cloud-enabled design allows us to perform smart design parameter selections, and reconfigurations for medical detection systems. Figure 6 and 7 demonstrate breast tissue density and its relationship with number of bits in pixel data presentation. Table 1 demonstrated Benchmark results. Column 1 listed the name of each test benchmark. Column 2 provides the resolution bits for each pixel in each test case. Column 3 gives the frame size for each image. Column 4 indicates the size of the biggest calcification cluster in each test case. Here, we have two cases without the number because the size of calcification cluster is negligible. Without the proposed design, the power per frame is listed in column 5. We also provided the power for each frame for the proposed method.

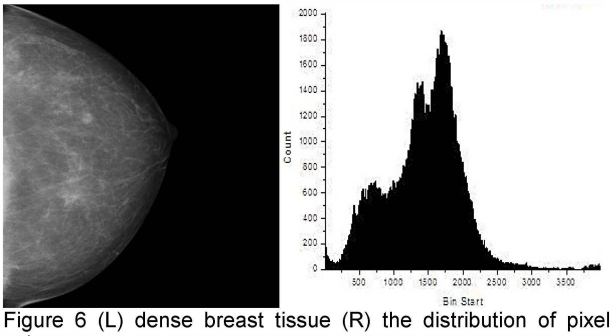

Figure 6 (L) dense breast tissue (R) the distribution of pixel values.

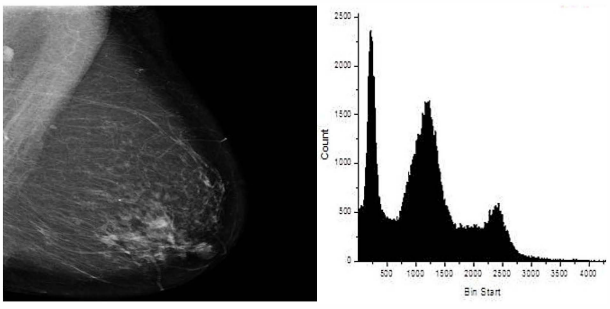

Figure 7: (L) Sparse breast tissue (R) the distribution of pixel values.

Unlike previous multiple read during integration (mrdi) scheme published by Boyd [16], we use only three sample image with reduce exposure time of T/16, T/8 and T/4 where T is integration time. We merge these three images by using the current High Dynamic Range Imaging approach. The final high dynamic Range image is creating with the estimate slope as in [16] and correction by Maximum A Posteriori (MAP) estimation with the prior is the probability density function (PDF) generates from the three lower exposed time images and the X-ray generating system model. Figure 7 shows the comparison between the images from our system and the original ones. And the reduction in X-ray dose 9/16. Furthermore, the estimate noise floor reduction is 20.8 times. We use UMC 90nm CMOS technology nodes. The whole design has 2.4 Ghz speed. The reconstructed image by the proposed idea for the 800x800 image shows a Power Signal Noise Ratio (PSNR) of 62.33 dB.

REFERENCES

1. P. Boyle and J. Ferlay. "Cancer incidence and mortality in Europe," 2004. Ann. Oncol., 16:481-488, 2005.
2. American Cancer Society, "Cancer Facts & Figure 2011."
3. European Hospital, "Digital mammography and tomosynthesis," December 31, 2007 http://www.european-hospital.com/en/article/3197-Digital_mammography_and_tomosynthesis.html
4. http://www.ucdmc.ucdavis.edu/radiology/research/boone3.html
5. Steve Si Jia Feng, Ioannis Sechopoulos," Clinical Digital Breast Tomosynthesis System: Dosimetric Characterization," Feb 13, 2012, DOI:10.1148/radiol.11111789 http://radiology.rsna.org/content/early/2012/02/09/radiol.11111789.full
6. A. Bandyopadhyay, J. Lee, R. W. Robucci, and P. Hasler, "Matia: A Programmable 80 uW/frame CMOS Block Matrix Transform Imager Architecture", IEEE Journal of Solid-State Circuits, Vol. 41, No. 3, March 2006. pp. 663-672.
7. A. Bandyopadhyay, P. Hasler, and D. Anderson, "ACMOSfloating-gate matrix transform imager," *IEEE Sensors*, vol. 5, no. 3, pp. 455–462, Jun. 2005.
8. S. Sugawa, N. Akahane, S. Adachi, K. Mori, T. Ishiuchi, and K. Mizobuchi, "A 100 dB dynamic range CMOS image sensor using a lateral overflow integration capacitor," in *IEEE ISSCC Dig. Tech. Papers*, Feb. 2005, pp. 352–353.
9. N. Akahane, S. Sugawa, S. Adachi, K. Mori, T. Ishiuchi, and K. Mizobuchi, "A sensitivity and linearity improvement of a 100-dB dynamic range CMOS image sensor using a lateral overflow integration capacitor," *IEEE J. Solid-State Circuits*, vol. 41, no. 6, pp. 851–858, Jun. 2006.
10. S. Adachi, S. Sugawa, N. Akahane, K. Mori, T. Ishiuchi, and K. Mizobuchi, "The tolerance for FD dark current and PD overflow current characteristics of wide dynamic range CMOS image sensor using a lateral overflow integration capacitor," in *Proc. IEEE Workshop on Charge-Coupled Devices and Advanced Image Sensors*, Jun. 2005, pp.153–156.
11. S. Adachi, W. Lee, N. Akahane, H. Oshikubo, K. Mizobuchi, and S. Sugawa, "A 200 uV/e CMOS Image Sensor With 100-ke Full Well Capacity", IEEE Journal of Solid-State Circuits, Vol. 43, No. 4, April 2008.
12. M. Lin, "Analogue to Information System based on PLL-based Frequency Synthesizers with Fast Locking Schemes", Ph.D thesis, The University of Edingburgh, Feb. 2010.
13. M. Schoberl, C. Senel, S. Fobel, H. Bloss and A. Kaup, "Non-linear Dark Current Fixed Pattern Noise Compensation For Variable Frame Rate Moving Picture Cameras", 17th European Signal Processing Conference (EUSIPCO 2009), August 24-28, 2009.
14. US patent 6674404 "Method and apparatus for error detection and correction in image sensor" Inventors: Suk Joong Lee, Gye Tae Hwang, Ichon-shi, Jan 6, 2004.
15. US patent 2009/0185636, "Parallel And Adaptive Signal Processing", Inventors: Zsolt Palotai, Veresegyhaz (HU) ; Andras Lorincs, Nagykovvacsi (HU).
16. Boyd Fowler," Low Noise Wide Dynamic Range Image Sensor Readout Multiple Reads During Integration (MRDI)," www.fairchildimaging.com/main/documents/mrdi.pdf
17. D. Donoho, "Compressive sensing," *IEEE Trans. on Inform. Theory*, vol. 52, no. 4, pp. 1289–1306, Sep 2006.
18. E. Candes, J. Romberg, and T. Tao, "Robust uncertainty principles: exact signal reconstruction from highly incomplete frequency information," *IEEE Trans. on Inform. Theory*, vol. 52, no. 2, pp. 489–509, Feb 2006.
19. R. Boufounos, R. G. Baraniuk, "Quantization of Sparse Representations," Data Compression Conference, p. 378, 2007.
20. R. Boufounos, R. G. Baraniuk, "Sigma Delta Quantization for Compressive Sensing." Proc. SPIE Waveletts XII. Proc. of SPIE Vol. 6701, 670104, (2007), doi: 10.1117/12.734880, August 26-29 2007, San Diego, CA.
21. D. Needell and J. A. Tropp, "CoSaMP: Iterative signal recovery from incomplete and inaccurate samples," Applied and Computational Harmonic Analysis, Vol. 26, No: 3, pp. 301-321, August 2009.

TestCase	Resol (#ofbits)	FrameSize (RowxCol)	CalSize (radius)	Old(w) /frame	New(w) /frame	Reduction OnPower%	Reduction on data %	NewSNR (db)
Dense_1	16	512x512	200um	1.58	1.14	28.37	32.189	93.5
Dense_2	16	800x800	N/A	2.43	1.65	32.4	43.54	80.13
Senior_1	12	512x512	N/A	0.96	0.624	34.5	69.2	89.21
Senior_2	12	800x800	3cm	1.57	0.858	45.3	57.3	92.14
Cancer_1	18	4800x6388	4cm	23.58	18.06	23.8	68.7	78.39
Cancer_2	18	2400x2400	5cm	17.33	11.43	34.3	53.5	75.24

Table 1 Test Benchmarks Comparison and Characteristics